Geophysical Research Letters

RESEARCH LETTER
10.1029/2022GL099277

Zeta Potential of a Natural Clayey Sandstone Saturated With Carbonated NaCl Solutions at Supercritical CO_2 Conditions

Miftah Hidayat[1,2], Mohammad Sarmadivaleh[2], Jos Derksen[1], David Vega-Maza[1,3], Stefan Iglauer[4,5], and Jan Vinogradov[1]

[1]School of Engineering, University of Aberdeen, Aberdeen, UK, [2]Curtin University, Discipline of Petroleum Engineering, Kensington, WA, Australia, [3]Now at University of Valladolid, School of Engineering. TermoCal, BioEcoUVa Institute, Valladolid, Spain, [4]Centre for Sustainable Energy and Resources, Edith Cowan University, Perth, WA, Australia, [5]School of Engineering, Edith Cowan University, Perth, WA, Australia

Key Points:

- First measurements of zeta potentials in an intact clayey sandstone saturated with CO_2-rich NaCl solutions at supercritical CO_2 conditions
- Zeta potential of clayey sandstone saturated with CO_2-rich NaCl is less negative compared with NaCl equilibrated with atmospheric CO_2
- The zeta potential of a clayey sandstone is more positive than that measured in a clean sandstone

Supporting Information:

Supporting Information may be found in the online version of this article.

Correspondence to:

M. Hidayat and J. Vinogradov,
miftah.hidayat.16@aberdeen.ac.uk;
jan.vinogradov@abdn.ac.uk

Citation:

Hidayat, M., Sarmadivaleh, M., Derksen, J., Vega-Maza, D., Iglauer, S., & Vinogradov, J. (2022). Zeta potential of a natural clayey sandstone saturated with carbonated NaCl solutions at supercritical CO_2 conditions. *Geophysical Research Letters*, *49*, e2022GL099277. https://doi.org/10.1029/2022GL099277

Received 29 APR 2022
Accepted 7 JUL 2022

Author Contributions:

Conceptualization: Jan Vinogradov
Data curation: Miftah Hidayat
Formal analysis: Miftah Hidayat, Jan Vinogradov
Investigation: Miftah Hidayat
Methodology: Jan Vinogradov
Project Administration: Mohammad Sarmadivaleh, Jan Vinogradov
Supervision: Mohammad Sarmadivaleh, Jos Derksen, David Vega-Maza, Stefan Iglauer, Jan Vinogradov
Validation: Miftah Hidayat, Jan Vinogradov

Abstract The zeta potential is a measure of electric potential at the mineral-electrolyte interfaces. The zeta potential of natural sandstones depends on mineralogy, electrolyte pH, concentration, composition, amount of dissolved CO_2, and temperature. We report for the first time the zeta potential measured on clayey sandstone comprising quartz, kaolinite, illite, albite and microcline saturated with NaCl solutions at supercritical CO_2 conditions. Our results demonstrate that zeta potentials in clayey sandstone samples at supercritical CO_2 conditions are significantly different from similar measurements conducted under ambient conditions and from those obtained with clean sandstones. Supercritical CO_2 zeta potential remains negative but is influenced by clays and feldspars due to their significant presence and exposure to large pores, which yields less negative zeta potential compared to quartz, under identical conditions. Our results have significant implications to natural subsurface systems such as CO_2 geo-sequestration sites, aquifers, geothermal sources and hydrocarbon reservoirs.

Plain Language Summary Sandstone is a type of porous rock commonly found in natural subsurface settings. Generally, the main mineral found in sandstone is quartz. However, other minerals such as clays and feldspars are also often present in sandstones. When the formation water flows through porous sandstone, the rock surface becomes electrically charged as water contacts minerals of the rock. The property that describes electrical properties of rock-water interface is termed the zeta potential, and it can be used to characterize subsurface flows and the wetting state of rocks. The zeta potential can be measured using the streaming potential method in the laboratory under conditions representative of subsurface systems. In this study we show that the zeta potential of clayey sandstone at supercritical CO_2 conditions is significantly different from the published data on clayey samples at ambient conditions and from clean sandstones comprising mostly quartz. Therefore, ignoring the effect of high content of dissolved CO_2 at high pressure and elevated temperature and the fact that other minerals in sandstone can modify the zeta potential might lead to misinterpretation of data and model estimates used a broad range of earth and environmental science applications.

1. Introduction

Zeta potential is a physicochemical property of interfaces between aqueous solutions (termed brines or electrolytes for simplicity) and minerals or other fluid phases. The mineral-brine zeta potential is interpreted from the measured streaming potential that arises due to pressure gradients in rocks saturated with electrolytes (Hunter, 1981; Jackson et al., 2012). Many experimental and modeling studies have reported the importance of the zeta potential for a broad range of applications for silica-brine systems, due to abundance of such formations. These applications include CO_2 geo-sequestration (CGS, e.g., Moore et al., 2004), hydrocarbon recovery (e.g., Jackson et al., 2016), geothermal resources (Jardani et al., 2008; Revil & Pezard, 1998), characterization of flow through fractured systems (Jougnot et al., 2020; Vinogradov et al., 2022), and management of groundwater aquifers (e.g., MacAllister et al., 2018).

The zeta potential of sandstone saturated with electrolytes at various conditions has been widely investigated experimentally covering high salinity (Walker & Glover, 2018), elevated temperature (Vinogradov & Jackson, 2015), multi-phase flows (Revil & Cerepi, 2004; Sprunt et al., 1994) and complex composition of brines

Visualization: Miftah Hidayat, Jan Vinogradov
Writing – original draft: Miftah Hidayat, Jan Vinogradov
Writing – review & editing: Miftah Hidayat, Jos Derksen, David Vega-Maza, Stefan Iglauer, Jan Vinogradov

(Thanh & Sprik, 2016). However, the only published data on zeta potentials of natural sandstones at CGS conditions (elevated temperature, high pore pressure, high CO_2 content) are limited to quartz dominated rock sample (Hidayat et al., 2022, hereafter referred to as H22), where measurements were carried out on a "clean" Fontainebleau (>99%wt quartz) sample at pore pressures up to 10 MPa and temperatures up to 40°C were reported. The authors found that the zeta potential remained negative, decreased with increasing content of dissolved CO_2, which resulted in a lower equilibrium pH. Many natural sandstone reservoirs comprise a broad range of various minerals, including clays, micas, feldspars and carbonates. These minerals are known to have a significant impact on the zeta potential (e.g., Hoxha et al., 2016; Peng et al., 2020) through the electrochemical interactions between individual minerals and ionic species at the mineral-water interface. These interactions result in establishment of micro-scale local zeta potentials for each mineral, which combined together define to the so-called effective or macro-scale zeta potential that is measured in cm-scale porous rocks with complex mineralogy (Collini & Jackson, 2022). The dependence of the macro-scale zeta potential on mineralogy of clayey sandstones under varying pore pressure, brine concentration and CO_2 content conditions, relevant to CGS remains largely unknown.

In the absence of experimental data of the zeta potential at such conditions, we report for the first time zeta potentials measured for a natural sandstone comprising quartz, feldspars, and clay minerals, in contact with CO_2-rich NaCl solutions. The experimental pore pressure and temperature conditions were varied between 0.2 and 10 MPa and between 23°C and 40°C, respectively. We demonstrate that the zeta potential response to varying pore pressure is unique and different from that of clean sandstone samples.

2. Materials and Methods

A cylindrical San Saba sandstone sample was used in this study. The petrophysical properties of the sample are provided in Table 1.

Prior to conducting the streaming potential measurements, the sample was cleaned following the procedure reported by Alroudhan et al. (2016) and at compatible with clay minerals conditions (see Supporting Information S1, and refer to McPhee et al., 2015). The porosity of the sample was measured using the gas (N_2) expansion method in AP-608 Automated Permeameter and Porosimeter (Coretest System Inc, USA). The liquid permeability and the formation factor (using NaCl solutions of concentration ranging between 0.05 and 1.0 M, M = mol/L) were calculated following the procedure reported in Vinogradov et al. (2010).

The experiments were conducted using NaCl aqueous solutions of varying ionic strength and were divided into two main groups corresponding to the electrolyte conditions: dead and live solutions. The former relates to a synthetic aqueous solution fully equilibrated with atmospheric CO_2, whereas the latter solution prepared under ambient pressure and temperature is brought into contact with pure CO_2 in a mixing reactor establishing thermodynamic equilibrium at elevated temperatures and pressures (for further details, refer to H22). To prepare dead and live electrolytes, we followed the experimental protocol reported by H22 to make sure the dead and live solutions reached full chemical equilibrium with the rock sample before the experiment commenced. The pH and conductivity of the dead electrolytes were regularly measured using a FiveGo pH meter (Mettler Toledo, accuracy of 0.01 pH units) and a Jenway 4520 conductivity meter (Cole-Palmer, 0.5% accuracy), respectively. Furthermore, an in-line high pressure pH meter (Corr Instruments, LLC) was used to measure pH of live electrolytes. The equilibrium pH and conductivity of all tested NaCl solutions are provided in Table 2.

The streaming potential measurements were conducted in a high pressure-high temperature (HPHT) coreflooding apparatus (see Figure 1 in H22). The streaming potential coupling coefficient (C_{SP}) was determined from the ratio between the stabilized voltage, ΔV, and the stabilized pressure difference, ΔP, across the sample following paired-stabilized method (Vinogradov & Jackson, 2011). We confirmed that the effect of surface conductivity was negligible in all our experiments (refer to Supporting Information S1) and therefore, the zeta potential (ζ) was calculated using the classical Helmholtz-Smoluchowski equation (Jouniaux & Pozzi, 1995) while disregarding the Overbeek's correction for the surface conductivity (Glover, 2015):

$$C_{SP} = \frac{\Delta V}{\Delta P} = \frac{\varepsilon \zeta}{\mu \sigma_w} \tag{1}$$

where $\varepsilon$is the electrolyte permittivity, μ is the electrolyte dynamic viscosity, and σ_w is the conductivity of the electrolytes (Table 1). The permittivity (ε) and dynamic viscosity (μ) of dead electrolytes were evaluated using

Table 1
Petrophysical and Mineralogical Properties of the San Saba Sample Used in This Study

Sample	San saba
Mineralogy	87.7% wt. – 95.2% wt. quartz
	2.3% wt. – 6.2% wt. microcline
	1.9% wt. – 4.0% wt. albite
	1.1% wt. – 3.3% wt. kaolinite
	0.9% wt. – 1.0% wt. illite
Porosity	21.0% ± 1.0%
Liquid permeability	35.0 ± 1.0 mD
Dimensions	Length = 7.61 cm
	Diameter = 3.82 cm
Formation factor, F	159 ± 8

Note. Mineralogy of the sample is provided as a range of the main constituents based on published studies of Connolly et al. (2019) and Al-Shajalee et al. (2020) and independently confirmed from X-ray diffraction and Scanning Electron Microscopy Analyses carried out in this study.

Table 2
The Equilibrium pH and Conductivity of Tested Electrolytes in This Study

Ionic strength, M	P, MPa	T, °C	Solution	σ_w, S/m	pH values
0.05	0.2	23	Dead	0.550	6.80 ± 0.1
	4.5			0.557	6.75 ± 0.1
	7.5			0.553	6.75 ± 0.1
	10.0			0.555	6.80 ± 0.1
	0.2	40		0.601	6.50 ± 0.1
	4.5			0.601	6.55 ± 0.1
	7.5			0.601	6.50 ± 0.1
	10.0			0.601	6.55 ± 0.1
	4.5		Live	0.505	3.72 ± 0.05
	7.5			0.496	3.43 ± 0.05
	10.0			0.493	3.26 ± 0.05
0.10	0.2	23	Dead	1.015	6.60 ± 0.1
0.20				1.982	6.60 ± 0.1
0.50				4.110	6.70 ± 0.1
1.00				8.090	6.70 ± 0.1

Note. P is the mean pore pressure which was kept 2–3 MPa below the confining pressure. T is the temperature during the experiment, which was controlled by the oven. The live electrolyte conductivity was evaluated using an empirical correlation reported by Börner et al. (2015).

an empirical correlation reported by Saunders et al. (2012). The dynamic viscosity of live electrolytes was calculated using the correlation reported by Islam and Carlson (2012).

3. Results

The zeta potentials measured with dead NaCl solutions of ionic strength between 0.05 and 1.0 M are shown in Figure 1. The zeta potential of San Saba remained negative and became larger in magnitude with increasing salinity until 0.2 M, after which it decreased back. This behavior contrasted most of previously published data obtained with sandstones containing other than quartz minerals (e.g., Stainton and St. Bees in Vinogradov et al., 2010 and Jaafar et al., 2009; Berea in Walker & Glover, 2018). However, a similar anomalous salinity dependence of the zeta potential was observed in Berea sandstones reported by Li et al. (2018) thus suggesting that our results were not an experimental artifact.

Figure 2 reports the measured zeta potentials and pH of dead (a–d) and live (e–f) solutions as a function of pore pressure and temperature. The results presented in Figures 2a and 2b demonstrate that the zeta potentials and pH of dead electrolytes remained independent of the pore pressure, similar to the results on Fontainebleau (H22). Note, that all dead electrolyte experiments were conducted in a closed system (Vinogradov et al., 2018), hence preventing contact with air and eliminating the possibility of enhanced dissolution of CO_2. Therefore, the amount of dissolved CO_2 and the electrolyte pH (Figure 2b) remained constant in all our dead electrolyte experiments, which resulted in the zeta potential to stay independent of the pore pressure.

The temperature dependence of the zeta potential and pH of dead electrolytes is shown in Figures 2c and 2d and compared with the published results for the clean Fontainebleau sample (H22). The zeta potential of dead electrolytes became smaller in magnitude with increasing temperature reflecting a decrease in pH of the solutions with increasing temperature. These observations were qualitatively consistent with published data on sandstones at elevated temperature (e.g., Vinogradov et al., 2018; H22). However, a weaker temperature dependence of zeta potential in San Saba was observed in comparison with Fontainebleau as evidenced by the slopes in Figure 2c (i.e., with the change in the experimental temperature from 23°C to 40°C, an increase of +2.0 mV was observed for the zeta potential in San Saba while a change of +4.3 mV was reported for Fontainebleau). Similarly, a smaller variation of the equilibrium pH of dead electrolytes saturating San Saba was observed with increasing temperature compared with the results reported for Fontainebleau (Figure 2d).

We finish by reporting the measured zeta potential and pH of live electrolytes in San Saba for three different pore pressure (4.5, 7.5 and 10 MPa) at 40°C with 0.05 M NaCl solutions (Figures 2e and 2f). The zeta potential of San Saba saturated with live solutions remained negative and became smaller in magnitude with increasing pressure (Figure 2e). The pH dependence of the zeta potential in San Saba was significantly different form that observed in Fontainebleau sample (H22) as evidenced by a distinct difference in respective slopes of the linear regressions. At the same time, the equilibrium pH of live electrolytes saturating San Saba decreased with increasing pressure at the same rate as that of Fontainebleau (Figure 2f) reflecting an increased amount of dissolved CO_2 that led to increased acidity of the electrolyte (Adamczyk et al., 2009; Peng et al., 2013).

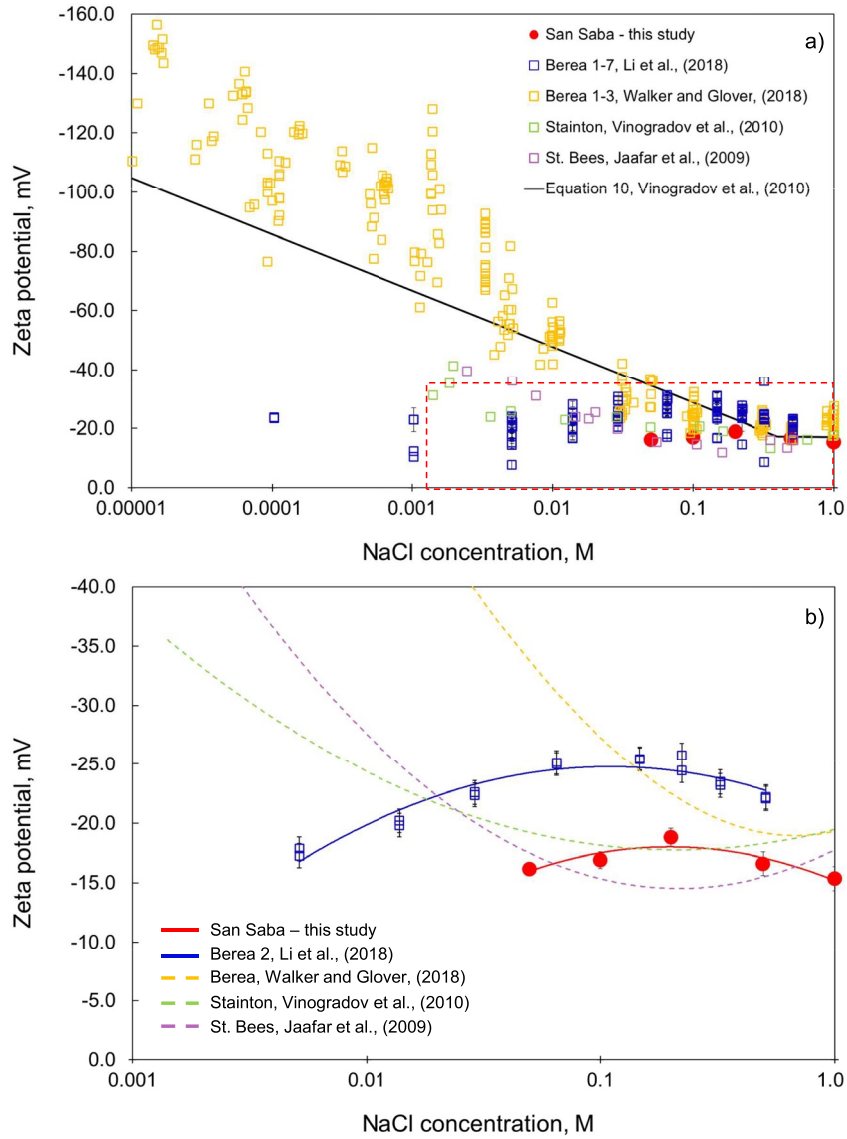

Figure 1. (a) The zeta potential of San Saba (red circles) compared with the published experimental data of clayey sandstones. The solid black line in (a) describes the empirical correlation published by Vinogradov et al. (2010). Panel (b) shows the same data as (a) but presents the averaged values of Jaafar et al. (2009), Vinogradov et al. (2010) and Walker and Glover (2018) described by respective trendlines over the salinity range between 0.001 and 1 M NaCl. The blue trendline corresponds to the experiment with Berea 2 sample from Li et al. (2018), while results for other Berea samples from the study are excluded since their salinity dependence of the zeta potential was qualitatively identical to the blue trendline but offset to larger or smaller in magnitude values. All trendlines in panel (b) are only used to qualitatively describe the salinity dependence of the zeta potential, thus they are based on polynomial regressions drawn through the respective excremental datapoints with $R^2 \geq 0.99$.

4. Discussion

A summary plot of the zeta potential as a function of pH for both live and dead NaCl solutions is presented in Figure 3. The zeta potentials of San Saba were found to be more positive compared with the values of clean Fontainebleau sandstone for live and dead NaCl electrolytes. We observed a steeper slope of zeta potential versus pH in San Saba (blue dashed line, Figure 3) compared with Fontainebleau (black dashed line, Figure 3) when the temperature changed from 23°C to 40°C for the dead electrolytes. Note, that the amount of dissolved CO_2 remained constant during these dead brine experiments at both temperatures. At the same time, a shallower slope of the zeta potential versus pH was observed in San Saba (purple dash line, Figure 3) saturated with live NaCl

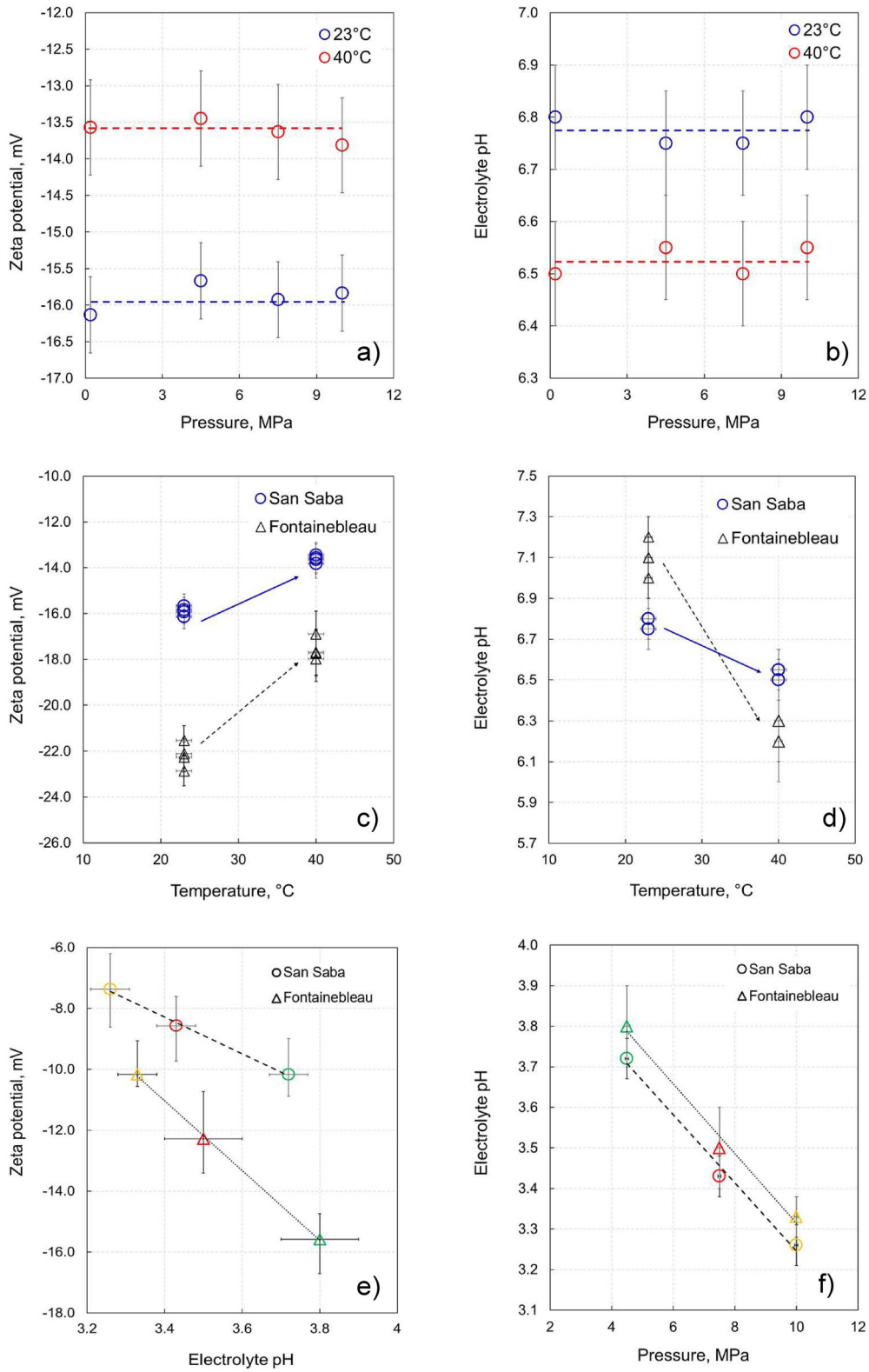
Zeta potential, mV
Pressure, MPa
23°C
40°C
a)
Electrolyte pH
b)
Temperature, °C
San Saba
Fontainebleau
c)
d)
e)
f)

Figure 2.

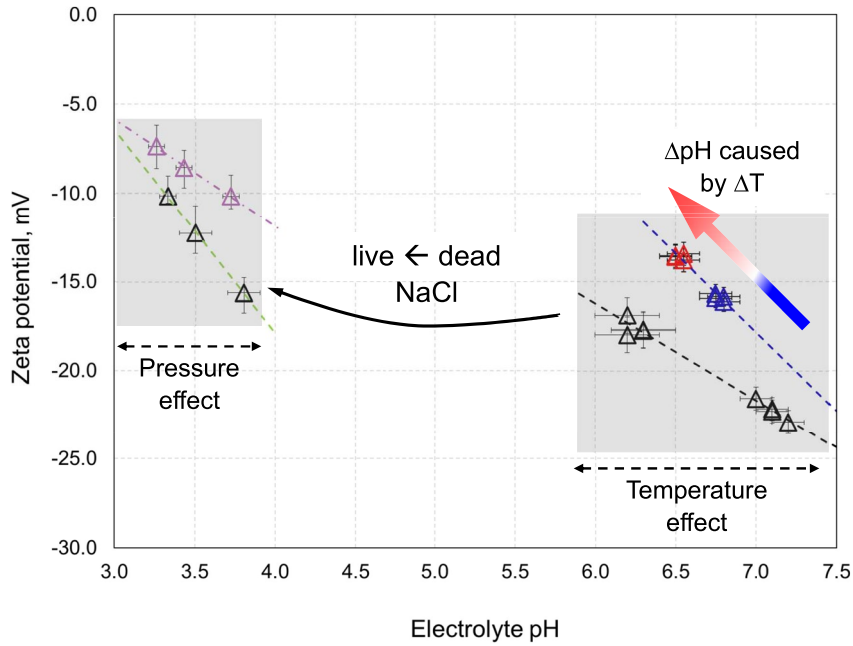

Figure 3. Summary of zeta potentials versus pH for dead and live electrolytes. The purple symbols correspond to live electrolytes; the blue and red symbols correspond to dead electrolytes at temperature of 23°C and 40°C, respectively. The previously published data for Fontainebleau sample saturated with dead and live NaCl solutions under the same experimental conditions are denoted by black symbols, and these values were extracted from H22.

solutions compared with Fontainebleau (green dashed line, Figure 3) over the range of tested experimental pore pressures between 4.5 and 10.0 MPa. Since the zeta potentials of San Saba and those of clean Fontainebleau samples were obtained under identical conditions of pore pressure, temperature and CO_2 content, we attributed differences in respective zeta potentials to the presence of clays and feldspars in San Saba.

A recently published study (Alarouj et al., 2021) suggested that the effective macro-scale zeta potential was an average of the micro-scale zeta potentials from each individual mineral-brine interface. That is, if the mineralogy of the rock sample was dominated by a single mineral such as quartz, then the micro- and macro-scale zeta potentials would be identical. If, on the other hand, various minerals were distributed along the pore walls, as in the case of San Saba sandstone, then the local micro-scale zeta potentials would vary from one mineral to another, and the macro-scale zeta potential would be an average of the micro-scale values depending on the portion of pore walls lined by different minerals.

To evaluate the impact of different minerals on the effective zeta potential of San Saba, additional investigations of the sample were carried out. From X-ray diffraction analysis (XRD), we found the mass fractions of minerals of the bulk sample, in which clays (kaolinite and illite), feldspars (albite and microcline) and quartz were identified as the main components (Table 1). However, the XRD analysis did not provide the necessary insights on how the identified minerals were distributed in the pore space. To address this question, we used the scanning electron microscopy (SEM), from which the same minerals were identified as the main constituents (Figure 4).

SEM image presented in Figure 4c identified a minor inclusion of chrome spinel, which appeared to be an extremely uncommon locality and was only found in a single spot of the thin section. Kaolinite and illite were found to extend toward the middle of large pores. Thus, kaolinite and illite were exposed to electrolyte during the streaming potential experiments and were expected to influence both micro- and macro-scale zeta potentials.

Figure 2. Zeta potential (a, c and e) and electrolyte *p*H (b, d and f) as a function of salinity, temperature and pore pressure. Zeta potentials (a) and pH (b) for the dead solutions were independent of pore pressure since the experiments were conducted in a closed system while the solutions were prepared with atmospheric level of CO_2 corresponding to partial CO_2 pressure of $10^{-3.44}$ atm (Li et al., 2016). Temperature dependence of the zeta potential (c) and pH (d) for dead solutions is compared with previously published data. Live brine zeta potential (e) and pH (f) are compared with previously published data. Green sybos correspond to pore (hence, partial CO_2) pressure of 4.5 MPa, red symbols stand for 7.5 MPa and yellow symbols denote experiments at 10 MPa. The Fontainebleau data presented in these figures were extracted from H22.

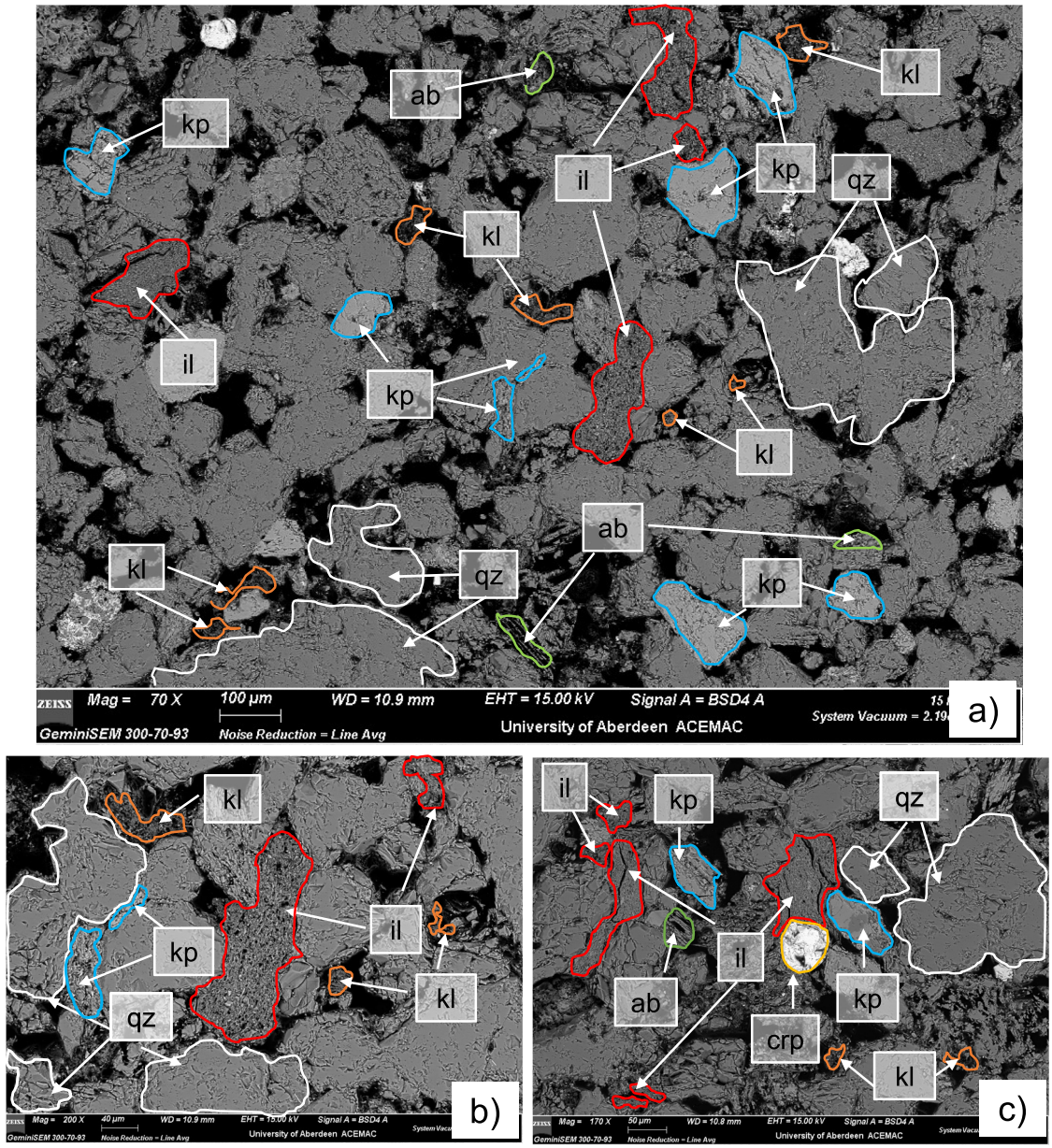

Figure 4. Images from scanning electron microscopy analysis of San Saba sandstone, in which the unmarked gray areas correspond to quartz. The abbreviations used in the figure are: qz for quartz, kl for kaolinite, ab for albite, il for illite, kp for K-feldspars (microcline), and crp for chrome spinel. The black color corresponds to pores in the rock sample.

Similar situation was observed with albite, which was found to extend toward major pores thus interacting with brines during the experiments (Figures 4a and 4c). Hence, albite was also expected to contribute to the overall macro-scale zeta potentials. On the other hand, the microcline grains were primarily locked between quartz grains (Figures 4a and 4b) or had a small area exposed to large pores (Figure 4c), thus limiting the mineral's interaction with electrolytes during the experiments. Therefore, the contribution of microcline to overall macro-scale zeta potentials was expected to be insignificant despite its relatively significant concentration of c. 2%–6%.

To understand the impact of each mineral, we compared the previously reported zeta potentials of the minerals with that of quartz. Yukselen-Aksoy and Kaya (2011) reported zeta potentials of kaolinite and quartz for pH range of 3–11 in water and found kaolinite zeta potentials to be less negative than quartz. Hussain et al. (1996) conducted zeta potential measurements with kaolinite and illite in water for pH range of 2.5–11 and found that the magnitude of illite zeta potentials was smaller than that of kaolinite. Furthermore, Wainipee et al. (2013)

measured zeta potentials of illite and kaolinite with 0.001 and 0.7 M NaCl and pH range of 1–9, and found that the zeta potentials of illite were less negative compared to kaolinite. Therefore, we concluded that the impact of kaolinite and illite on the negative zeta potentials should lead to the following relative magnitudes $|\zeta_{illite}| < |\zeta_{kaolinite}| < |\zeta_{quartz}|$, all shifting the macro-scale zeta potential of San Saba to more positive values compared with clean Fontainebleau.

A study by Vidyadhar and Rao (2007) reported that microcline zeta potential was more negative than quartz in water for pH range of 1.5–11. On the other hand, the zeta potential of albite was measured to be less negative than quartz in water for pH range of 1.5–11 (Vidyadhar et al., 2002; Wang et al., 2018). Demir et al. (2001) investigated the effect of ionic strength of NaCl electrolytes on the zeta potentials of albite and microcline over a wide salinity range (0.0001–0.1M NaCl), and found that zeta potential in albite was less negative compared to microcline. Based on these findings, we concluded that the magnitude of the negative zeta potential of albite is the smallest, followed by quartz and microcline ($|\zeta_{albite}| < |\zeta_{quartz}| < |\zeta_{microcline}|$).

Numerous experimental studies investigated dissolution of kaolinite and albite, and the dissolution rates were reported to increase with increasing temperature and decreasing pH (Cama et al., 2002; Carroll & Walther, 1990; Harley & Gilkes, 2000; Palandri & Kharaka, 2004). Thus, we hypothesize that kaolinite, albite and illite dissolved during our experiments releasing multi-valent cations such as Ca^{2+}, Mg^{2+}, Al^{3+} (Cama et al., 2002; Li et al., 2018; Yuan & Pruett, 1998), which caused their adsorption and/or exchange at the quartz surface of San Saba making the zeta potential more positive, as was suggested by published studies of the zeta potential on clayey sandstones (Alarouj et al., 2021; Li et al., 2018).

All in all, based on the bulk composition (Table 1) and pore-scale distribution of main minerals of San Saba (Figure 4) we concluded that the main impact on the macro-scale zeta potential came from kaolinite and albite, both of which had higher presence in the bulk (c. 1%–3% wt. and 2%–4% wt., respectively), and larger available surface area for interactions between ionic species of brines and minerals (i.e., substantial exposure of mineral surfaces to pore fluid in larger pores). Conversely, a smaller amount of illite (c. 1% wt.) and limited exposure to flowing brines of microcline made their contribution to the macro-scale zeta potential negligible. The experimental results of this study confirmed the hypothesized individual contribution of minerals and demonstrated that both, kaolinite and albite of San Saba made the effective macro-scale zeta potentials in this study more positive compared with Fontainebleau (H22). Moreover, these minerals were more reactive with NaCl solutions thus making the pH dependence of the zeta potential significantly different compared with quartz data across the tested range of pH and temperature (Figure 3).

5. Conclusions

We report for the first time zeta potentials measured on intact clayey San Saba sandstone sample saturated with NaCl solutions of various concentrations and under conditions of temperature, pH, dissolved CO_2 content and pore pressure consistent with CGS. The zeta potential of San Saba was negative for all tested solutions, but when in contact with live electrolytes it decreased in magnitude with increasing pore pressure due to increased amount of dissolved CO_2 and the corresponding decrease in pH. Conversely, the zeta potential of San Saba and dead electrolytes was found to be independent of the pore pressure condition but decreased with increasing temperatures reflecting respective changes in pH. Furthermore, the zeta potential with both, dead and live solutions was less negative when compared with previous experimental and modeling studies of clean sandstones at similar conditions. An anomalous salinity dependence of the zeta potential was observed with dead NaCl of ionic strength 0.05–1.0 M, which is uncommon but qualitatively similar to the previously reported data on a different clayey sandstone (Li et al., 2018).

We found that mineralogy of San Saba played a key role in defining the micro- and macro-scale zeta potentials. Specifically, a larger content of kaolinite and albite combined with their substantial presence in large pores made these minerals to chemically interact with flowing brines, which led to a smaller in magnitude macro-scale zeta potential compared with that of pure quartz. Furthermore, increased dissolution rate of kaolinite, illite and albite at elevated temperature and low pH (around 3) likely resulted in appearance of multi-valent cations in the electrolyte, which further led to specific adsorption and/or ion exchange at the mineral surface, eventually leading to smaller in magnitude zeta potentials compared with quartz-NaCl systems. On the other hand, microcline, mostly locked between quartz grains, and small concentration of illite in San Saba did not have noticeable impact on

the macro-scale zeta potential. Our results demonstrate that mineralogy of sandstones has a noticeable impact on electrochemical interactions at the mineral-brine interface and must be investigated to predict and explain the salinity, composition, pH and temperature dependence of the effective macro-scale zeta potentials.

The results of this study are novel and essential for a broad range of applications including underground gas storage (CO_2/H_2), monitoring of subsurface flows, geothermal sources and hydrocarbon recovery. However, additional measurements of zeta potentials are required and planned to investigate the effect of electrolyte composition, concentration, pore pressure, temperature and CO_2 content over extended ranges and in other clayey sandstone samples.

Data Availability Statement

Detailed information on rock sample preparation and petrophysical characterization is available for download in the Supporting Information S1. Summarized experimental data of San Saba sandstone in this study is available for download at https://doi.org/10.5281/zenodo.6477225.

Acknowledgments
Miftah Hidayat was supported by the Aberdeen-Curtin PhD studentship. David Vega-Maza is funded by the Spanish Ministry of Science, Innovation and Universities ("Beatriz Galindo Senior" fellowship BEAGAL18/00259). Abbie McLaughlin from School of Natural and Computing Sciences and John Still from the School of Geoscience, University of Aberdeen are acknowledged for their assistance in the XRD and SEM analyses.

References

Adamczyk, K., Prémont-Schwarz, M., Pines, D., Pines, E., & Nibbering, E. T. (2009). Real-time observation of carbonic acid formation in aqueous solution. *Science*, *326*(5960), 1690–1694. https://doi.org/10.1126/science.1180060

Alarouj, M., Collini, H., & Jackson, M. D. (2021). Positive zeta potential in sandstones saturated with natural saline brine. *Geophysical Research Letters*, *48*(20), e2021GL094306. https://doi.org/10.1029/2021GL094306

Alroudhan, A., Vinogradov, J., & Jackson, M. D. (2016). Zeta potential of intact natural limestone: Impact of potential-determining ions Ca, Mg and SO_4. *Colloids and Surfaces A: Physicochemical and Engineering Aspects*, *493*, 83–98. https://doi.org/10.1016/j.colsurfa.2015.11.068

Al-Shajalee, F., Arif, M., Sari, A., Wood, C., Al-Bayati, D., Xie, Q., & Saeedi, A. (2020). Low-salinity-assisted cationic polyacrylamide water shutoff in low-permeability sandstone gas reservoirs. *Energy & Fuels*, *34*(5), 5524–5536. https://doi.org/10.1021/acs.energyfuels.0c00022

Börner, J. H., Herdegen, V., Repke, J. U., & Spitzer, K. (2015). The electrical conductivity of CO_2-bearing pore waters at elevated pressure and temperature: A laboratory study and its implications in CO_2 storage monitoring and leakage detection. *Geophysical Journal International*, *203*(2), 1072–1084. https://doi.org/10.1093/gji/ggv331

Cama, J., Metz, V., & Ganor, J. (2002). The effect of pH and temperature on kaolinite dissolution rate under acidic conditions. *Geochimica et Cosmochimica Acta*, *66*(22), 3913–3926. https://doi.org/10.1016/S0016-7037(02)00966-3

Carroll, S. A., & Walther, J. V. (1990). Kaolinite dissolution at 25 degrees, 60 degrees, and 80 degrees C. *American Journal of Science*, *290*(7), 797–810. https://doi.org/10.2475/ajs.290.7.797

Collini, H., & Jackson, M. D. (2022). Relationship between zeta potential and wettability in porous media: Insights from a simple bundle of capillary tubes model. *Journal of Colloid and Interface Science*, *608*, 605–621. https://doi.org/10.1016/j.jcis.2021.09.100

Connolly, P. R., Yan, W., Zhang, D., Mahmoud, M., Verrall, M., Lebedev, M., et al. (2019). Simulation and experimental measurements of internal magnetic field gradients and NMR transverse relaxation times (T2) in sandstone rocks. *Journal of Petroleum Science and Engineering*, *175*, 985–997. https://doi.org/10.1016/j.petrol.2019.01.036

Demir, C., Abramov, A. A., & Çelik, M. S. (2001). Flotation separation of Na-feldspar from K-feldspar by monovalent salts. *Minerals Engineering*, *14*(7), 733–740. https://doi.org/10.1016/S0892-6875(01)00069-3

Glover, P. W. J. (2015). Geophysical properties of the near surface Earth: Electrical properties. In *Treatise on Geophysics*, In G. Schubert (Ed.) (2nd edn). (Vol. 11, pp. 89–137). Elsevier. https://doi.org/10.1016/B978-0-444-53802-4.00189-5

Harley, A. D., & Gilkes, R. J. (2000). Factors influencing the release of plant nutrient elements from silicate rock powders: A geochemical overview. *Nutrient Cycling in Agroecosystems*, *56*(1), 11–36. https://doi.org/10.1023/A:1009859309453

Hidayat, M., Sarmadivaleh, M., Derksen, J., Vega-Maza, D., Iglauer, S., & Vinogradov, J. (2022). Zeta potential of CO_2-rich aqueous solutions in contact with intact sandstone sample at temperatures of 23°C and 40°C and pressures up to 10.0 MPa. *Journal of Colloid and Interface Science*, *607*, 1226–1238. https://doi.org/10.1016/j.jcis.2021.09.076

Hoxha, B. B., Sullivan, G., Van Oort, E., Daigle, H., & Schindler, C. (2016). Determining the zeta potential of intact shales via electrophoresis. In *SPE Europec featured at 78th EAGE conference and exhibition*, OnePetro. https://doi.org/10.2118/180097-MS

Hunter, R. J. (1981). *Zeta potential in colloid science: Principles and applications*. Academic press.

Hussain, S. A., Demirci, Ş., & Özbayoğlu, G. (1996). Zeta potential measurements on three clays from Turkey and effects of clays on coal flotation. *Journal of Colloid and Interface Science*, *184*(2), 535–541. https://doi.org/10.1006/jcis.1996.0649

Islam, A. W., & Carlson, E. S. (2012). Viscosity models and effects of dissolved CO_2. *Energy & Fuels*, *26*(8), 5330–5336. https://doi.org/10.1021/ef3006228

Jaafar, M. Z., Vinogradov, J., & Jackson, M. D. (2009). Measurement of streaming potential coupling coefficient in sandstones saturated with high salinity NaCl brine. *Geophysical Research Letters*, *36*(21), L21306. https://doi.org/10.1029/2009GL040549

Jackson, M. D., Gulamali, M. Y., Leinov, E., Saunders, J. H., & Vinogradov, J. (2012). Spontaneous potentials in hydrocarbon reservoirs during waterflooding: Application to water-front monitoring. *SPE Journal*, *17*(01), 53–69. https://doi.org/10.2118/135146-PA

Jackson, M. D., Vinogradov, J., Hamon, G., & Chamerois, M. (2016). Evidence, mechanisms and improved understanding of controlled salinity waterflooding part 1: Sandstones. *Fuel*, *185*, 772–793. https://doi.org/10.1016/j.fuel.2016.07.075

Jardani, A., Revil, A., Bolève, A., & Dupont, J. P. (2008). Three-dimensional inversion of self-potential data used to constrain the pattern of groundwater flow in geothermal fields. *Journal of Geophysical Research*, *113*(B9), B09204. https://doi.org/10.1029/2007JB005302

Jougnot, D., Roubinet, D., Guarracino, L., & Maineult, A. (2020). Modeling streaming potential in porous and fractured media, description and benefits of the effective excess charge density approach. In *Advances in modeling and interpretation in near surface geophysics* (pp. 61–96). https://doi.org/10.1007/978-3-030-28909-6_4

Jouniaux, L., & Pozzi, J. P. (1995). Streaming potential and permeability of saturated sandstones under triaxial stress: Consequences for electrotelluric anomalies prior to earthquakes. *Journal of Geophysical Research*, *100*(B6), 10197–10209. https://doi.org/10.1029/95JB00069

Li, S., Collini, H., & Jackson, M. D. (2018). Anomalous zeta potential trends in natural sandstones. *Geophysical Research Letters*, *45*(20), 11–068. https://doi.org/10.1029/2018GL079602

Li, S., Leroy, P., Heberling, F., Devau, N., Jougnot, D., & Chiaberge, C. (2016). Influence of surface conductivity on the apparent zeta potential of calcite. *Journal of Colloid and Interface Science*, *468*, 262–275. https://doi.org/10.1016/j.jcis.2016.01.075

MacAllister, D. J., Jackson, M. D., Butler, A. P., & Vinogradov, J. (2018). Remote detection of saline intrusion in a coastal aquifer using borehole measurements of self-potential. *Water Resources Research*, *54*(3), 1669–1687. https://doi.org/10.1002/2017WR021034

McPhee, C., Reed, J., & Zubizarreta, I. (2015). Core sample preparation. In *Developments in petroleum science*. (Vol. 64, pp. 135–179). Elsevier. https://doi.org/10.1016/b978-0-444-63533-4.00004-4

Moore, J. R., Glaser, S. D., Morrison, H. F., & Hoversten, G. M. (2004). The streaming potential of liquid carbon dioxide in Berea sandstone. *Geophysical Research Letters*, *31*(17). https://doi.org/10.1029/2004GL020774

Palandri, J. L., & Kharaka, Y. K. (2004). A compilation of rate parameters of water-mineral interaction kinetics for application to geochemical modeling. *US Geological Survey*. https://doi.org/10.3133/ofr20041068

Peng, C., Crawshaw, J. P., Maitland, G. C., Trusler, J. M., & Vega-Maza, D. (2013). The pH of CO2-saturated water at temperatures between 308 K and 423 K at pressures up to 15 MPa. *The Journal of Supercritical Fluids*, *82*, 129–137. https://doi.org/10.1016/j.supflu.2013.07.001

Peng, R., Di, B., Glover, P. W., Wei, J., Lorinczi, P., Liu, Z., & Li, H. (2020). Seismo-electric conversion in shale: Experiment and analytical modelling. *Geophysical Journal International*, *223*(2), 725–745. https://doi.org/10.1093/gji/ggaa288

Revil, A., & Cerepi, A. (2004). Streaming potentials in two-phase flow conditions. *Geophysical Research Letters*, *31*(11), a–n. https://doi.org/10.1029/2004GL020140

Revil, A., & Pezard, P. A. (1998). Streaming electrical potential anomaly along faults in geothermal areas. *Geophysical Research Letters*, *25*(16), 3197–3200. https://doi.org/10.1029/98GL02384

Saunders, J. H., Jackson, M. D., Gulamali, M. Y., Vinogradov, J., & Pain, C. C. (2012). Streaming potentials at hydrocarbon reservoir conditions. *Geophysics*, *77*(1), E77–E90. https://doi.org/10.1190/geo2011-0068.1

Sprunt, E. S., Mercer, T. B., & Djabbarah, N. F. (1994). Streaming potential from multiphase flow. *Geophysics*, *59*(5), 707–711. https://doi.org/10.1190/1.1443628

Thanh, L. D., & Sprik, R. (2016). Zeta potential in porous rocks in contact with monovalent and divalent electrolyte aqueous solutions. *Geophysics*, *81*(4), D303–D314. https://doi.org/10.1190/geo2015-0571.1

Vidyadhar, A., & Rao, K. H. (2007). Adsorption mechanism of mixed cationic/anionic collectors in feldspar-quartz flotation system. *Journal of Colloid and Interface Science*, *306*(2), 195–204. https://doi.org/10.1016/j.jcis.2006.10.047

Vidyadhar, A., Rao, K. H., & Forssberg, K. S. E. (2002). Adsorption of n-tallow 1, 3-propanediamine–dioleate collector on albite and quartz minerals, and selective flotation of albite from greek stefania feldspar ore. *Journal of Colloid and Interface Science*, *248*(1), 19–29. https://doi.org/10.1006/jcis.2001.8174

Vinogradov, J., Hidayat, M., Kumar, Y., Healy, D., & Comte, J.-C. (2022). Laboratory measurements of zeta potential in fractured Lewisian gneiss: Implications for the characterization of flow in fractured crystalline bedrock. *Applied Sciences*, *12*(1), 180. https://doi.org/10.3390/app12010180

Vinogradov, J., Jaafar, M. Z., & Jackson, M. D. (2010). Measurement of streaming potential coupling coefficient in sandstones saturated with natural and artificial brines at high salinity. *Journal of Geophysical Research*, *115*(B12), B12204. https://doi.org/10.1029/2010JB007593

Vinogradov, J., & Jackson, M. D. (2011). Multiphase streaming potential in sandstones saturated with gas/brine and oil/brine during drainage and imbibition. *Geophysical Research Letters*, *38*(1). https://doi.org/10.1029/2010GL045726

Vinogradov, J., & Jackson, M. D. (2015). Zeta potential in intact natural sandstones at elevated temperatures. *Geophysical Research Letters*, *42*(15), 6287–6294. https://doi.org/10.1002/2015GL064795

Vinogradov, J., Jackson, M. D., & Chamerois, M. (2018). Zeta potential in sandpacks: Effect of temperature, electrolyte pH, ionic strength and divalent cations. *Colloids and Surfaces A: Physicochemical and Engineering Aspects*, *553*, 259–271. https://doi.org/10.1016/j.colsurfa.2018.05.048

Wainipee, W., Cuadros, J., Sephton, M. A., Unsworth, C., Gill, M. G., Strekopytov, S., & Weiss, D. J. (2013). The effects of oil on as (V) adsorption on illite, kaolinite, montmorillonite and chlorite. *Geochimica et Cosmochimica Acta*, *121*, 487–502. https://doi.org/10.1016/j.gca.2013.07.018

Walker, E., & Glover, P. W. J. (2018). Measurements of the relationship between microstructure, pH, and the streaming and zeta potentials of sandstones. *Transport in Porous Media*, *121*(1), 183–206. https://doi.org/10.1007/s11242-017-0954-5

Wang, W., Cong, J., Deng, J., Weng, X., Lin, Y., Huang, Y., & Peng, T. (2018). Developing effective separation of feldspar and quartz while recycling tailwater by HF pretreatment. *Minerals*, *8*(4), 149. https://doi.org/10.3390/min8040149

Yuan, J., & Pruett, R. J. (1998). Zeta potential and related properties of kaolin clays from Georgia. *Mining, Metallurgy & Exploration*, *15*(1), 50–52. https://doi.org/10.1007/BF03402787

Yukselen-Aksoy, Y., & Kaya, A. (2011). A study of factors affecting on the zeta potential of kaolinite and quartz powder. *Environmental Earth Sciences*, *62*(4), 697–705. https://doi.org/10.1007/s12665-010-0556-9%23